HHS Public Access

Author manuscript

*FEBS Lett*. Author manuscript; available in PMC 2021 November 30.

Published in final edited form as:

*FEBS Lett*. 2021 April ; 595(7): 925–941. doi:10.1002/1873-3468.14052.

# Flexibility and Adaptability in Pleiotrophin's Interactions with Glycosaminoglycans

**Eathen Ryan**, **Shen Di**, **Wang Xu***

School of Molecular Sciences, Arizona State University, Tempe, Arizona, U. S. A.

## Abstract

Pleiotrophin (PTN) is a potent mitogenic cytokine whose activities are controlled by its interactions with glycosaminoglycan (GAG). We examined PTN's specificity for several types of GAG oligosaccharides. Our data indicated PTN's interaction with GAGs is dependent on the sulfation density of GAGs. Surprisingly, an acidic peptide also had similar interactions with PTN as GAGs. This shows PTN's interaction with anionic polymers is flexible and adaptable and the charge density is the main determinant of the interaction. In addition, we showed that PTN can compensate for the loss of its termini in interactions with heparin oligosaccharides, allowing it to maintain its affinity for GAGs in their absence. Taken together, these data provide valuable insight to PTN's interactions with its proteoglycan receptors.

### Keywords

Pleiotrophin; Glycosaminoglycan; NMR; PTPRZ

## Introduction

Pleiotrophin (PTN) is a potent mitogenic and angiogenic cytokine capable of modulating a broad spectrum of physiological processes, including neural development [1–3], tissue repair [4–7], cell differentiation [8–10], inflammation [11], angiogenesis [12–16], and cancer [17–19]. The mechanisms by which PTN effects all of its activities are complex and, in many cases, still not well understood. But it is recognized that PTN's wide ranging activities are connected with its ability to bind a diverse collection of receptors. These receptors include receptor type protein tyrosine phosphatase ζ (PTPRZ) [20], syndecan [21], glypican [1], nucleolin [22], as well as β2 and β3 integrins [23,24]. A large proportion of the PTN receptors are proteoglycans, i.e. glycoproteins that carry the sulfated polysaccharide glycosaminoglycan (GAG). PTN is an avid binder of GAG, and its interactions with GAG are crucial to its activity.

GAG is a family of large, linear, and complex polysaccharides known to control many cellular processes. GAGs are composed of repeating disaccharide units and are classified based on the composition of their disaccharide repeats. PTN's affinity is highest for sulfated GAGs, which usually contain disaccharide units consisting of one amino sugar and one

*Corresponding author, xuwang@asu.edu.

uronic acid. The amino sugar can be either an N-acetylglucosamine (GlcNAc) or an N-acetylgalactosamine (GalNAc), and the uronate can be either a glucuronate (GlcA) or an iduronate (IdoA). Among the most common sulfated GAGs, chondroitin sulfate (CS) contains the disaccharide (3GalNAcβ1–4GlcAβ1) while dermatan sulfate (DS) contains the disaccharide (3GalNAcβ1–4IdoAα1). Heparin and heparan sulfate contain a mixture of (4GlcNAcα1–4IdoAα1) and (4GlcNAcα1–4GlcAβ1). Despite the simplicity of their carbohydrate backbones, GAG structures can be exceedingly complex. This is mainly because GAGs can be enzymatically sulfated in a semi-random fashion. In particular, GalNAc in CS and DS can be sulfated at the 4-O- and 6-O- positions. IdoA in DS, heparin, and HS can be 2-O-sulfated. GlcNAc in heparin and HS are often N-sulfated after N-deacetylation, producing GlcNS. 6-O-sulfation occurs in both GlcNAc and GlcNS and 3-O-sulfation in GlcNS is also common. Because the sulfation pathway is template-independent and influenced by both enzyme specificity and substrate availability, the resulting sulfation pattern is complex and potentially unique to each GAG polysaccharide [25]. However, the sulfation pattern on a GAG is integral to its activity since sulfation pattern is a critical determinant of protein-GAG interactions. Some GAG-binding proteins are known to recognize specific sulfation motifs in GAG. For instance, antithrombin is highly selective for the pentasaccharide GlcNS6S-GlcA-GlcNS6S3S-IdoA2S-GlcNS6S, which binds to antithrombin through an uncommon trisulfated monosaccharide GlcNS6S3S [26]. However, determining whether a protein recognizes specific sulfation motifs is still challenging. PTN is known to bind both CS proteoglycan (PTPRZ) and HS proteoglycans (syndecans and glypican), but whether PTN recognizes specific GAG classes or GAG sulfation motifs has not been thoroughly investigated.

PTN's structure is composed of two pseudo thrombospondin type 1 repeat (TSR) domains, referred to as the N-terminal domain (NTD) and the C-terminal domain (CTD), flanked by two unstructured termini. Both the structured domains and the termini are highly enriched in basic amino acids. Basic amino acid clusters in the structured domains of PTN include R52 and K54 on the NTD as well as K60 and K61 in the linker between the TSR domains. The CTD also has two basic amino acid clusters: cluster 1 consists of K84, R86, and K107 while cluster 2 consists of K68, K91, and R92. Previous characterization of PTN-GAG interactions showed that PTN binds to unfractionated GAG with a *K*d in the nM range [27]. Both TSR domains interact with heparin and both are necessary to achieve a high affinity for unfractionated heparin [28,29]. Other studies showed that CS oligosaccharides containing at least eighteen monosaccharides (dp18) are needed to achieve significant affinity [30]. However, a hexasaccharide consisting of the highly sulfated GalNAc4S-IdoA2S disaccharide units, common in DS, has also been shown to be a potent binder of PTN in competition assays [31]. In our previous work, we investigated the CS-A (GalNAc4S-GlcA) and CS-E (GalNAc6S4S-GlcA) binding sites on the protein [32]. We showed CS-E binding perturbed mostly residues in basic amino acid cluster two of the C-terminal TSR domain (CTD) (K68, K91, and R92) and the linker connecting the two TSR domains. In addition, its affinity for CS-A is significantly lower than CS-E and the C-terminus is required to bind CS-A, but not the highly sulfated CS-E [32].

Despite decades of work on PTN-GAG interactions, two crucial questions remain unanswered: (1) Do PTN interact differently with different GAG types? (2) Do different

domains of PTN bind GAG co-operatively? Although our previous work has examined interactions of PTN with CS while others have studied heparin, a systematic examination of PTN's interactions with the major GAG types under uniform conditions has not been undertaken. In addition, none of investigations used structurally homogeneous GAG oligosaccharides, a deficiency that may have prevented the identification of GAG motifs specifically recognized by PTN. Lack of information on PTN's GAG specificity has hampered the understanding of the structure-activity relationship of PTN-GAG interactions. It also means the most optimal GAG ligands for studying PTN may not be used in biochemical characterizations of PTN-GAG interactions. Knowing the GAG-binding cooperativity among PTN's domains will similarly provide significant insight into PTN-GAG interactions and facilitate structural studies of PTN-GAG complexes by reducing the complexity in the system. In the current work, we investigated these questions using a combination of solution NMR and isothermal titration calorimetry (ITC) experiments. Specifically, we systematically investigated whether different types of sulfated GAG interact with PTN differently and how different PTN domains contribute to GAG binding. Our data show that heparin, CS-E, DS, and CS-A oligosaccharides induced perturbations in a similar set of PTN residues. However, the magnitudes of chemical shift perturbation are highly-dependent on sulfation density of the GAG. This trend was also observed in a set of paramagnetic relaxation enhancement (PRE) experiments carried out with three structurally homogeneous heparin hexasaccharides, which all perturbed a similar set of residues but the magnitudes of PRE increased with the sulfation density of the hexasaccharide. These data indicate charge density plays an important role in PTN's interactions with its ligands. Consistent with that conclusion is the observation that an acidic peptide derived from the stem region of PTPRZ binds PTN with a similar affinity and produces similar perturbations in PTN as GAG oligosaccharides, a sign that the main GAG binding site of PTN does not discriminate among anionic polymers. A global comparison of all chemical shift perturbation data was also carried out using principal component analysis (PCA). Classification of the titration data using the principal components generated three major groups that are separated by charge density. This confirms the observation that charge density is the major determinant in PTN's interaction with anionic polymers. In regard to the contribution of each PTN domain to GAG binding, our data show that the flanking basic termini do contribute to the binding of highly sulfated GAG such as heparin. Specifically, our NMR data show there are significant NOEs between GAG and Lysines in these termini. Moreover, in the absence of the termini, the TSR domains' GAG affinity increased, allowing PTN to maintain its affinity for GAG even in the absence of the termini. In addition, although separation of the TSR domains did not affect each domains' affinity for short heparin oligosaccharides, the magnitudes of chemical shift perturbations were less for some residues. These results show PTN has a considerable amount of redundancy and flexibility in its interactions with GAG and other anionic molecules, which may be a significant reason for its pleiotropy.

## Materials and Methods

### Generation of truncated PTN mutants.

Wild type PTN and its truncation constructs were generated from the open reading frame of human wild type PTN acquired from DNASU (dnasu.asu.edu). The mature wild type PTN contained residues 1 to 136. N-terminus truncated PTN (PTN-ΔN) contained residues 13 to 136. C-terminus truncated PTN (PTN-ΔC) contained residues 1 to 114. Dual N/C-termini truncated PTN (PTN-ΔNC) contained residues 13 to 114. NTD and CTD were produced by adding ORF coding residues 1 to 57 or 58 to 114 of PTN to the 3' end of 6His-tagged ubiquitin ORF in the plasmid pHUE [33].

### Expression and purification of wild type PTN and structural variants.

The wild type and terminally truncated PTN constructs were cloned into pET-15b vector, and subsequently transformed into Origami B (DE3) (Novagen) for bacterial expression. All protein expression was achieved by growth in M9 medium, either as unlabeled or supplemented with $^{15}NH_4Cl$ and/or $^{13}C$-glucose for isotopically labeled protein, at 37°C to an $OD_{600}$ between 0.5–0.8. This was followed by overnight induction with 0.25mM IPTG at 23°C. Cell pellets were harvested via centrifugation before resuspended in 20 mM Tris (pH 7.5), 200 mM NaCl, and 2.5% glycerol. Cell lysis was performed by a combination of 1 mg/mL of lysozyme and sonication. Protein extraction from the supernatant was done through cation-exchange chromatography with a 5 mL HiTrap SP column (GE Life Sciences) with 20 mM Tris (pH 7.5), 200 mM NaCl, and 2.5% glycerol as the equilibration buffer, and protein was eluted using a NaCl gradient of 0.2 M to 1.5 M. Single domain PTN variants were cloned into pHUE vector [33] as a fusion protein with His-tagged ubiquitin, and transformed into Origami B (DE3) (Novagen) for bacterial expression. The same growth and expression conditions were used as in truncated and wild type PTN. However, protein purification was done through $Ni^{2+}$-affinity chromatography with a 5 mL HisTrap column (GE Life Sciences). Bound PTN domains were eluted by applying an imidazole gradient of 35 to 500 mM. After exchanging the pooled protein into 25 mM Tris and 100 mM NaCl buffer (pH 8.0), the fusion protein was cleaved with 1/20 molar equivalent of the deubiquitinase USP2 overnight at room temperature [33]. Another $Ni^{2+}$-affinity column was applied to separate cleaved PTN domains from His-tagged ubiquitin and His-tagged USP2 enzyme.

### Expression and purification of the PTPRZ peptide.

The sequence corresponding to PTPRZ residues G1414 to K1441 (GGGEDGDTDDDGDDDDDDRGSDGLSIHK) was cloned into the pHUE vector [33] as a C-terminal fusion with the His-tagged ubiquitin using SacII and HindIII restriction sites. The plasmid was transformed into BL21(DE3) for recombinant expression. In particular, the cells were grown in LB media and induced by adding 0.5 mM IPTG when $OD_{600}$ reached 0.8. The culture was then incubated at room temperature overnight. To purify the protein, the His-tagged fusion protein was extracted by $Ni^{2+}$-affinity chromatography, and the His-tagged ubiquitin was separated from the PTPRZ peptide by digestion using the USP2 deubiquitinase [33]. The His-tagged ubiquitin was removed by passing the digested

mixture through $Ni^{2+}$-affinity column. The final product was confirmed using tricine SDS-PAGE electrophoresis and NMR.

### Generation of GAG fragments.

Heparin, DS, and CS-A (Sigma-Aldrich) were digested through enzymatic depolymerization with Heparinase I for heparin, and Chondroitinase ABC for both CS-A and DS until depolymerization was approximately 30% complete, as indicated by the $A_{232nm}$ absorbance. Digested fragments were separated via size exclusion chromatography on a 2.5 cm × 175 cm column packed with Bio-Rad Biogel P10 resin and run at a flow rate of 0.2 ml/min. Heparin oligosaccharides were further separated through SAX HPLC to produce structurally homogenous fragments of different sulfation density.

### Semi-synthesis of chondroitin sulfate E.

Chondroitin sulfate E (CS-E) was synthesized through chemical sulfation of CS-A according the procedure in Cai et al.[34] Briefly, 3.5 g of CS-A was dissolved in 90 mL of formamide with 5 g of trimethylamine sulfur trioxide. The reaction was stirred vigorously and kept at 60° C under $N_2$ gas for 24 hours. After completion of the reaction, the product was dialyzed for two days in water before lyophilization. CS-E hexasaccharides (dp6) were obtained by digesting CS-E using Chondroitinase ABC (Sigma Aldrich) and purified using the size exclusion chromatography procedure described above.

### Paramagnetic labeling of oligosaccharides.

Structurally homogenous heparin dp6 were conjugated to TEMPO through reductive amination of the sugars. Each 0.5 mg of hexasaccharide was reductively aminated with 0.3 M 4-amino-TEMPO using 20 mM $NaCNBH_3$ as the reducing agent in a 400 uL total reaction volume. Labeling reactions were carried out with neutral pH for two days, so as not to reduce the free radical. The reaction temperature was 65°C. All reactions were subsequently desalted to remove excess TEMPO.

### Titrations of PTN variants.

Wild type PTN and variants were titrated with enzymatically digested heparin dp6, CS-E dp6, CS-A octasaccharides (dp8) and DS dp8. Titrations were carried out on a Bruker Avance III 600 MHz spectrometer or Varian Inova 800 MHz spectrometer. Wild type PTN was titrated with heparin dp6 by adding aliquots of a 33.3 mM stock to the protein to final heparin dp6 concentrations of 0, 0.05, 0.1, 0.2, 0.4, 0.6, 0.8, and 1 mM. The protein concentration was 125 μM. Titration of wild type PTN with CS-E dp6 was performed by adding aliquots of 40 mM CS-E dp6 stock solution to a 125 μM PTN sample to produce final CS-E dp6 concentrations of 0.125, 0.375, 0.625, 0.875, and 1.125 mM. CS-A dp8 titration was carried out at concentrations of 0, 0.09, 0.26, 0.51, 0.77, 1.11, 1.45, and 1.87 mM ligand in a 400 uL sample containing 190 uM wild type PTN. Stock concentration of CS-A dp8 was 90 mM. DS dp8 titration was performed using a sample of 200 uM PTN, with titration points at 0, 0.2, 0.4, 0.4, 0.8, 1.2, 1.6 and 2.0 mM DS dp8. DS dp8 stock solution contained 80 mM DS dp8. Titrations of wild type PTN with structurally homogeneous heparin dp6 fragments (DP6-1, DP6-2, and DP6-3) were performed with 50

μM protein and ligand stock concentrations of 10.5 mM, 15 mM, and 12.5 mM for DP6-1, DP6-2, and DP6-3, respectively. Aliquots of the high purity heparin dp6 fragments were added to reach ligand concentrations of 0, 0.025, 0.05, 0.075, 0.1, 0.2, 0.3, 0.4, and 0.5 mM. All titrations were carried out in 10 mM MES, pH 6.0, 150 mM NaCl. To titrate PTN's NTD and CTD with heparin dp6, aliquots of heparin dp6 were added to samples of 100 μM NTD or CTD until the heparin dp6 concentrations were 0, 0.05, 0.1, 0.2, 0.4, 0.6, and 0.8 mM. To titrate wild type PTN with the PTPRZ peptide, six separate samples were prepared. Samples contained 50 μM of $^{15}$N-labeled PTN and 0, 25, 50, 100, 150, and 200 μM of the PTPRZ peptide, respectively. To titrate wild type PTN and PTN-ΔNC with heparin dp8, aliquots of heparin dp8 were added to a 100 μM PTN or PTN-ΔNC sample until the heparin dp8 concentration was either 0, 0.05, 0.1, 0.2, 0.4, 0.6, and 0.8 mM. PTN- ΔC samples were also titrated with CS-E dp6 and CS-A dp8 using identical parameters for the titrations of wild type PTN with the same ligands. For all titrations, a $^{15}$N-edited HSQC spectrum was collected at each titration point, and proton chemical shifts were referenced to internal DSS, with $^{15}$N resonances referenced indirectly to DSS using absolute frequency ratios. Observed chemical shift changes were measured and the normalized Eulidean distance was calculated using the equation: $\delta = [\Delta\delta H^2 + (0.17 \times \Delta\delta N)^2]^{1/2}$, where ΔδH and ΔδN represent chemical shift changes in the $^1$H and $^{15}$N dimensions in ppm. *K*d values were calculated by fitting plots of normalized chemical shift changes vs. ligand concentration using the one-to-one binding model fitting feature in xcrvfit (http://www.bionmr.ualberta.ca/bds/software/xcrvfit/).

### Measurements of heparin dp6-induced paramagnetic relaxation enhancements on PTN.

To measure the paramagnetic contribution to the transverse relaxation rates of PTN amide protons ($R_{2,PRE}$) as a result of PTN's interactions with TEMPO-labeled DP6-1, DP6-2, and DP6-3 hexasaccharides, 0.25 molar equivalents of TEMPO-labeled heparin hexasaccharides was added to 300 μL of 300 μM PTN. The paramagnetic contribution to the transverse relaxation was measured as the difference between amide proton transverse relaxation rates ($R_2$) before and after the reduction of the TEMPO radical. Reduction of TEMPO was achieved through addition of 10 molar equivalencies of ascorbate (pH 6.0).

### Global comparison of chemical shift perturbation datasets using PCA.

To compare chemical shift perturbation patterns of different titrations in a global and quantitative manner, PCA was applied to chemical shift changes from ten sets of titrations. The titrations included wild type PTN titrated with heparin dp6, CS-E dp6, DS dp8, CS-A dp8, DP6-1, DP6-2, DP6-3, and the PTPRZ peptide. PTN-ΔC (residues 1 to 114) titrated with CS-E dp6 and CS-A dp8 were also included. PCA was carried out on $^1$H and $^{15}$N chemical shift changes in ppm units individually with $^{15}$N chemical shift changes being scaled by a factor of 0.17. Only residues whose chemical shift changes in all the titrations were used. The data were analyzed using the pca function in Matlab. Clustering of the observations in the score plot was done using the kmeans function in Matlab.

### Collection and analysis of intermolecular contact data.

Intermolecular contact data for PTN was collected on a Bruker 850 MHz Avance III HD spectrometer equipped with a cryoprobe. F3-filtered/F1-$^{13}$C-edited NOESY was collected

on 0.2 mM of $^{13}C/^{15}N$-labeled wild type PTN in the presence of 0.8 mM of the heparin hexasaccharide DP6-3. The mixing time was 0.2 s. All data processing was performed with NMRPipe [35] and analyzed using NMRView.[36]

### Isothermal titration calorimetry.

ITC of wild type and truncated PTN with heparin dp8 was performed on a Microcal ITC-200 calorimeter. Samples consisting of 300 μL of 100 μM PTN were titrated with aliquots of 3 mM heparin dp8 stock solution at 25°C. Buffer containing no protein was used as a reference. Each titration was repeated two times, and average values of the dissociation constants and enthalpy change are reported.

### Modeling of the PTN-GAG complex.

To create a model of the PTN-GAG complex based on the available data, AMBER14 parameters for a heparin dp12 consisted of only the disaccharide unit (4-6-O-sulfo-GlcNSα1-4-2-O-sulfo-IdoAα1) was created using the Glycam force field [37,38]. The oligosaccharide was docked onto the GAG-binding site consisting of the linker, CTD's basic amino acid cluster 2 (K68, K91, and R92), and NTD residues Q51, R52, and K54 using ambiguous distance constraints between GlcNS.H2 and GlcNS.H3 and side chains of the aforementioned basic amino acids. The constraints were designed to place the reducing end of the oligosaccharide near cluster 2 of CTD and the non-reducing end of the oligosaccharide near cluster 1 of CTD. Only the structured portion of PTN (residues 13 to 114) was used in the docking. The docked structures were visually inspected, and distance constraints were adjusted to optimize the matching between the basic amino acid clusters and the GlcNS residues in the oligosaccharide. To ensure the complex structure is stable, the best structure was subjected to 450 ns of unconstrained MD to allow the complex to reach equilibrium.

## Results

### Perturbations of heparin, CS-E, DS, and CS-A on PTN.

Although PTN has a high affinity for several types of GAGs [27,29], it is unclear whether it interacts with all GAG types in the same way. To determine this, we applied the technique of chemical shift perturbation mapping, which is commonly used to analyze protein-GAG interactions [39,40], to compare the effect of heparin hexasaccharides (dp6), CS-E dp6, DS octasaccharides (dp8), and CS-A dp8 on PTN. Figures 1 and S1 show the superimposition of $^{15}N$-edited HSQC spectra of $^{15}N$-labeled PTN in the presence of different concentrations of these oligosaccharides. Similar to previous studies [29,32], residues in the linker bridging CTD and NTD (residues 58 to 67) as well as residues around basic amino acid cluster 2 of CTD (residues 68 to 70 and 90 to 100) experienced the largest chemical shift perturbations. A comparison of the migration directions of the signals showed the perturbations in different titrations were mostly comparable (Figures 1 and S2). This indicates PTN's binding site and interaction with each GAG are similar. However, whereas heparin, CS-E, and DS oligosaccharides elicited large chemical shift changes in the spectrum of PTN, chemical shift changes produced by CS-A were modest. Moreover, fitting the migration curves of residues N96 from the CTD and T34 from the NTD using a one-to-one binding model

showed heparin dp6 and CS-E dp6 have the highest affinity for PTN. This was followed by DS dp8 while CS-A dp8 has the lowest affinity. The variations in the *K*ds of different oligosaccharides can be mostly explained by differences in the sulfation densities of GAGs. In particular, heparin, which has the highest sulfation density, also has the highest PTN affinity. Although DS and CS-A nominally have similar sulfation densities, disaccharide analysis showed that ~ 10 % of DS disaccharides contain a higher number of sulfates whereas higher sulfation disaccharides were negligible in CS-A (Figure S3). This means more than 40 % of DS dp8 may contain at least one oversulfated disaccharide. This may explain DS dp8's higher affinity for PTN than CS-A dp8. Consistent with previous studies [29,32], the GAG affinity of the CTD is higher than the GAG affinity of the NTD.

### Interactions of PTN with structurally defined heparin dp6 oligosaccharides.

Because the oligosaccharides used in the aforementioned experiments were a heterogeneous mixture, the detected perturbations reflect only the average for all oligosaccharides. Therefore, information on specific interactions with distinct oligosaccharides may be lost as a result of averaging. To investigate whether PTN is capable of recognizing specific structural features in oligosaccharides, we purified three highly sulfated heparin dp6 oligosaccharides to structural homogeneity so their interactions with PTN can be studied. The three hexasaccharides, designated as DP6-1 (ΔUA2S-GlcNS6S-IdoA-GlcNAc6S-GlcA-GlcNS6S3S), DP6-2 (ΔUA2S-GlcNS6S-IdoA2S-GlcNS6S-GlcA-GlcNS6S), and DP6-3 (ΔUA2S-GlcNS6S-IdoA2s-GlcNS6S-IdoA2s-GlcNS6S) (structures are shown in Figure S4), differ both in the number of sulfate groups and their carbohydrate backbones. We titrated PTN with each oligosaccharide. The results show that they perturbed PTN in a similar manner and the *K*ds of their interactions with PTN were also very similar (Figures 2A and 2C). All three have slightly higher affinities for PTN than heparin dp6 mixtures, which may reflect the fact that heparin dp6 mixtures used in this study likely contained a high fraction of low sulfation density oligosaccharides.

It has been shown that subtle changes in GAG's sulfation pattern may change the binding orientation without changing the binding site [41]. To investigate whether this is the case with the three hexasaccharides, we conjugated 4-amino-TEMPO to the reducing end of the hexasaccharides and used the paramagnetically-tagged hexasaccharides to probe PTN. Paramagnetic centers broaden NMR signals of nearby atoms in a distance-dependent fashion. The resulting paramagnetic relaxation enhancement (PRE) is commonly used to identify ligand binding sites in proteins [42]. By conjugating the TEMPO to the reducing end through reductive amination, we can identify the binding orientation for the oligosaccharide by measuring changes in the transverse relaxation rate ($R_2$) of amide protons before and after the radical on the oligosaccharide is reduced to a hydroxide. Figure 2B shows the PRE's contribution of these TEMPO-labeled heparin dp6 oligosaccharides to the backbone amide proton $R_2$ ($R_{2,PRE}$). Similar to the chemical shift perturbation results, residues experiencing large $R_{2,PRE}$ were centered around the linker (residues 58 to 68) and CTD's basic amino acid cluster 2 (residues 68 to 70 and 90 to 100). Signals of several residues in these regions, including Q51, C53, C57, N58, W59, F63, Y69, and F71, were broadened beyond detection in the presence of oxidized radical and only reappeared after the radical was reduced. These residues are indicated by an asterisk in

Figure 2B. In addition, residues 28 to 33 in the NTD also showed significant PRE. Unlike the aforementioned segments in the CTD, these NTD residues did not experience large chemical shift perturbation, but their proximity to the linker and CTD means they are close to the GAG-binding site, therefore their perturbation is not unexpected given the sensitivity of PRE. One notable feature in the PRE results is that hexasaccharides with more sulfate groups generated significantly stronger PRE to residues around cluster 2 than those with fewer sulfate groups. This observation is analogous to the large chemical shift perturbations produced by highly sulfated GAGs and is most likely a reflection of PTN's preference for highly sulfate GAG oligosaccharides.

Another notable feature is that DP6-3 induced significant NMR signal broadening in the linker residues, preventing them from being analyzed. Such signal broadenings were observed with other heparin oligosaccharide ligands. Because GAG is known to induce the oligomerization of midkine, a cytokine highly homologous to PTN [43], we examined whether heparin dp6 oligosaccharides used in this study are capable of producing stable PTN oligomers using size exclusion chromatography (SEC) and glutaraldehyde crosslinking. Figure S5A shows the SEC chromatograms of PTN in the presence and absence of heparin dp6 oligosaccharides. It is clear that no oligomers of PTN can be observed, but a small shoulder whose molecular weight is similar to a one-to-one complex of PTN and heparin dp6 can be seen. This shows stable PTN oligomers cannot be isolated. We also carried out glutaraldehyde crosslinking to detect the existence of transient oligomers. This experiment showed that chemical crosslinking of PTN in the presence of heparin dp6 oligosaccharides did increase the fraction of cross-linked oligomers (Figure S5B). These results imply that, at the concentration of PTN and heparin dp6 oligosaccharides used in the NMR study, transient oligomerization of PTN is possible. Therefore, the observed NMR signal broadening is likely caused by the formation of these oligomers.

### PTN's interaction with acidic peptides.

The correlation between GAG charge density and PTN interaction prompted us to explore whether non-glycan anionic polymers are also capable of interacting with PTN. To test this idea, we investigated PTN's interaction with an acidic peptide derived from the stem region of PTPRZ. In particular, residues G1414 to K1441 of PTPRZ (sequence: GGGEDGDTDDDGDDDDDDRGSDGLSIHK) contain a high concentration of aspartate and glutamate. If PTN's interaction with ligands is governed simply by electrostatics, then this peptide should mimic GAG's interactions with PTN. Interaction between PTN and this segment of PTPRZ may also be functionally relevant since it is known that PTPRZ core protein is still capable of binding PTN in the absence of GAG [20]. Interaction between PTN and this region of PTPRZ may explain such observations. To test how this anionic peptide binds PTN, we titrated $^{15}$N-labeled PTN with the peptide consisting of residues G1414 to K1441. Figure 3 shows the superimposition of the $^{15}$N-HSQCs of PTN in the presence of different concentrations of the peptide. Remarkably, the chemical shift migration pattern is almost identical to that produced by GAG oligosaccharides. The peptide also bound PTN with a *K*d of ~ 30 μM for residues in the CTD of PTN, similar to heparin dp6. These results confirm PTN uses the same binding site for all anionic linear polymers. However, it should be noted that the peptide induced smaller magnitude migrations than heparin dp6.

### PCA analysis of ligand-induced chemical shift changes.

Although visual inspections of the chemical shift perturbation patterns indicate the main difference in perturbations produced by different ligand lies mostly in the magnitudes of the perturbations, unique but subtle spectral changes may still exist. The existence of such features would indicate that the ligands' interactions with PTN are more specific than originally thought. To identify these possible features, we used PCA to analyze commonalities and differences in chemical shift perturbation patterns of these titrations. Data from all the titrations above as well as CS-E dp6 and CS-A dp8 titrations of a truncated PTN variant (PTN-ΔNC, residues 1 to 114) were used in the analysis. The input data consisted of changes in $^{1}H$ and $^{15}N$ chemical shifts in ppm units and only data from residues whose chemical shift perturbations can be measured in all titrations were used in the analysis. In addition, chemical shift changes of $^{15}N$ atoms were scaled by a factor of 0.17, similar to the scaling factor used in chemical shift mapping. In most titrations, the ratio of protein-to-ligand is ~ 1:10. One exception is the titration of PTN by the PTPRZ peptide, which only reached a protein-to-ligand ratio of ~ 1:4.2 due to the limited quantity of peptide available. However, the binding curve shows protein is close to being saturated (Figure 3C). Therefore, the chemical shift changes should be close to the maximum changes. Overall, data from 75 residues were used in the analysis and all of whom are located in the structured domains of PTN. PCA of the data was carried out in a manner similar to the procedure outlined in the work of Van Doren and colleagues [44]. The result showed that one principal component (PC1) alone is sufficient to account for ~ 80 % of the variance, indicating the titrations produced similar perturbations. Figure 4A shows the coefficients of PC1. The shape of the graph follows closely the chemical shift perturbation mappings shown in Figures 1, 2, and 3. The second largest principal component (PC2) only accounts for ~ 8 % of the variance. Score plot of different titration datasets along the two largest principal components is shown in Figure 4B. Clustering of the data sets using the K-means algorithm grouped titrations of CS-A dp8 and the PTPRZ peptide into one cluster, titrations of CS-E dp6 and DS dp8 into another cluster while all the heparin titrations fall into a third cluster. This clustering is consistent with the charge density of the ligands. In particular, CS-A has only 1.0 negative charge per sugar residue, while CS-E and DS can average 1.5 negative charges per sugar residue, and heparin is known to have 2.0 negative charges per sugar residue. The distance between amino acids in an unstructured peptide is ~ 3.5 Å, which is similar to the size of a monosaccharide. This means the charge density of a string of aspartate or glutamate should be similar to CS-A. Therefore, the analysis confirms that charge density is the most important feature in determining the chemical shift perturbations of a ligand on PTN.

### Cooperativity of PTN's TSR domains in GAG binding.

Another important question is whether the two TSR domains bind GAG oligosaccharide cooperatively. Raulo et al. showed that, although separated TSR domains can still bind unfractionated heparin, their GAG affinities are significantly weaker than intact PTN [45]. In a separate study, Solera et al., using a combination of experimental data and modeling, proposed that the two TSR domains in midkine, a protein highly homologous to PTN, bind short GAG oligosaccharides cooperatively [46]. However, there is yet no experimental evidence to show this is the case for PTN. We investigated the problem by examining

whether the separation of the TSR domains changes the interactions of each domain with GAG. Cooperative binding requires both domains, therefore separating the domains should lead to a dramatic decrease in each domain's affinity for GAG. Figure 5 shows $^{15}$N-HSQCs of wild type PTN, NTD, and CTD. In agreement with a previous study [45], separation of the domains produced negligible changes in the HSQCs of the domains, an indication that the structures of the domains are independent of each other. Separation of the domains also did not affect each domain's affinity for heparin dp6 as judged by the binding curves of T34 from the NTD and N96 from the CTD. However, the magnitudes of chemical shift perturbations of both residues were smaller than in the wild type protein. Several residues in the NTD, such as C32 showed no heparin-induced perturbation at all in the absence of CTD even though the residue showed significant perturbation in the wild type protein (Figure 5A). In addition, residue T38 showed slightly larger heparin-induced perturbation in the separated NTD than in wild type protein. This shows that, although the individual TSR domains are still able to bind GAG oligosaccharides independently, their interactions with GAG may not be identical to the wild type protein. Therefore, the domains do influence each other's interactions with GAG to some extent.

### Contributions of the termini to GAG binding.

PTN is a highly basic protein and its TSR domains are not the only basic segments. In particular, its unstructured termini are also enriched in basic amino acids. Although the termini are not necessary for binding highly sulfated GAG such as heparin or CS-E, they are essential to binding low sulfation density GAG such as CS-A [32]. However, despite conclusive evidence that shows the removal of termini does not affect heparin binding [32,45], $^{13}$C/$^{15}$N-filtered/$^{13}$C-edited NOESY experiments designed to isolate intermolecular contacts between $^{13}$C,$^{15}$N-labeled PTN and various heparin oligosaccharides produced only intermolecular NOEs between the oligosaccharides and Lysines whose chemical shifts are typical of Lysines in the unstructured termini of PTN (Figure S6). This prompted us to reexamine the termini's contributions to heparin binding. To do this, we prepared truncation mutants of PTN missing either the C-terminus (residues 115 to 136), the N-terminus (residues 1 to 12), or both. We then analyzed the affinity of these PTN mutants for heparin dp8 using both NMR and isothermal titration calorimetry (ITC). The two techniques are complimentary as multidimensional NMR allows the local GAG affinity of each domain to be measured whereas ITC is reflective of the overall GAG affinity of PTN. ITC also offers the entropic and enthalpic break down of the the binding free energy, providing further insight into the binding mechanism. Table 1 and Figure S7 show ITC measurements of the mutants' affinity for heparin dp8. Consistent with previous studies, the removal of the termini did not change the *K*d of the interaction at all. However, upon closer examination, it can be seen that, although wild type PTN's binding of heparin dp8 is driven mainly by entropic contributions, removal of the C-terminus or both the N- and C-termini have resulted in a change in the thermodynamics of the binding. In particular, the enthalpic contribution of the binding has increased significantly upon the removal of the termini. These changes signify that removing the termini has changed the interaction between PTN and heparin dp8 without changing the overall affinity. Additional evidence of the changes in PTN-heparin interactions comes from NMR titrations. Figure 6 shows $^{15}$N-HSQCs acquired during heparin dp8 titrations of wild type PTN and truncated PTN missing both termini. The

binding curves derived from these data show both CTD and NTD experienced significant enhancement in their affinity for GAG after the termini were removed. This indicates that CTD and NTD may be playing a greater role in GAG binding in the absence of the termini. This compensatory mechanism may explain the lack of changes in heparin affinity of PTN after the removal of the termini, even though the termini show signs of heparin binding.

## Discussion

Results in this study revealed a complex picture of PTN's interaction with GAGs. First of all, PTN's interactions with GAG oligosaccharides are highly flexible and adaptable. In particular, both GAGs and acidic peptides produced similar perturbation patterns in the NMR spectra of PTN. This implies PTN uses the same binding site for all anionic polymers and the charge density on the ligands appears to be the largest factor in determining the strength of their interaction with PTN. The biophysical basis for PTN's flexibility and adaptability in ligand interaction still requires further investigation, but the fact that PTN's basic amino acid clusters are enriched with Lysines, which have highly flexible side chains, may be a significant factor to its adaptability for different anionic ligands. Functionally, this flexibility may be one of the reasons for PTN's promiscuity for receptors and the source of its pleiotropy. In particular, PTN's affinity for the acidic PTPRZ peptide may explain the experimental observation that PTN can bind the PTPRZ core protein in the absence of GAG [20]. This indicates there may be non-glycan PTN binding sites in PTPRZ. The results presented here show the segment G1414 to K1441 is a potential PTN binding site in the PTPRZ core protein. However, given the acidic nature of PTPRZ's stem region, this may not be the only binding site for PTN.

The adaptable nature of PTN's interactions with ligands does not necessarily mean it has no specificity at all. In particular, the magnitudes of PRE produced by TEMPO-labeled oligosaccharides on residues close to CTD's cluster 2 were different and roughly correlate with the sulfation density of the oligosaccharides. This implies that cluster 2 may have a preference for motifs with higher sulfation density. However, further elucidation of this specificity will require more structurally homogeneous oligosaccharides or the use of GAG microarray. It should also be noted that PTN may show more specificity for ligands of larger size because the ability of longer GAG oligosaccharides to span both PTN domains may require a more specific sulfation pattern. Such an investigation is not currently possible because longer heparin oligosaccharides induce protein precipitation and NMR signal broadening, rendering the complexes inaccessible to high-resolution NMR characterization.

Flexibility and adaptability also characterize how the domains of PTN interact with ligands. Our data show that NTD and CTD retain their affinity for short heparin oligosaccharides, but changes in chemical shift perturbations indicate their interactions with GAG may not be the same as in the intact protein. Therefore, the domains do influence each other's interaction with GAG, albeit to a limited extent. In addition, there is evidence that the TSR domains do cooperatively bind longer GAG chains. In particular, separating the domains decreased PTN's affinity for unfractionated heparin by more than 100 times, a clear sign that cooperative binding is in play [29]. One surprising observation is that, despite the domains' relative independence in binding short oligosaccharide ligands, the stoichiometry of binding

calculated from ITC is always one-to-one and all NMR chemical shift perturbations were linear, which are also indicative of one-to-one binding. However, these observations do not completely eliminate the possibility that multiple GAG oligosaccharides may bind to the same PTN molecule. In particular, it is possible that the relative independence of the two domains means that GAG-binding in one domain does not influence chemical shifts of atoms in the neighboring domain, thereby preventing NMR from detecting formation of ternary complexes. In addition, ITC may only detect GAG-binding to one site if GAG interaction in the second site does not contribute to enthalpic changes. This is possible because electrostatic interactions do not result in enthalpic changes in Gibbs free energy [47,48] and protein-GAG interactions rely heavily on electrostatic interactions. Another possiblility is that heparin dp8, which was used in ITC experiments, is able to bind both domains simultaneously as a result of its larger size whereas the smaller heparin dp6, whch was used to study ligand binding cooperativity between the domains, cannot. This will then allow only one heparin dp8 to bind each PTN in the ITC titrations whereas two heparin dp6 may bind each PTN in the NMR titrations.

Besides the TSR domains, this study also showed the unstructured termini have a significant influence on the binding of highly sulfated GAG even though their absence does not change PTN's affinity for highly sulfated GAGs. The study was prompted by the detection of intermolecular NOEs between GAG and Lysines in unstructured termini. ITC results show that, although removing the termini does not change the overall affinity of PTN for GAG, it does change the binding mechanism. In particular, binding of wild type PTN is mostly driven by favorable entropic changes, whereas removal of the termini shifted the binding to a mechanism that is driven by favorable enthalpic changes. The change in the binding mechanism was supported by NMR data, which showed removing the termini increased the TSR domains' affinity for GAG oligosaccharides. These results showed that PTN's multiple GAG binding sites allow it to retain GAG affinity without the termini. C-terminus-free PTN has been observed in cellular assays [49]. The results from this study may help to elucidate the mechanism by which these truncated PTN variants retain their affinity for highly sulfated GAG, and point to potential ways by which PTN maintains its activity in important biological processes.

The considerable amount of structural data reported here consistently point to two sites in PTN as having the largest GAG-induced perturbation. Specifically, both the linker residues (residues 58 to 68) and residues around basic amino acid cluster 2 of CTD (residues 90 to 100) are heavily perturbed in both chemical shift mapping and PRE. PRE also indicates NTD residues adjacent to the linker and CTD (residues 51 to 57) as being close to the GAG-binding sites. These three segments are adjacent to each other and contain a significant number of basic amino acids. Although a single heparin dp6 oligosaccharide is not large enough to cover all three sites, a heparin oligosaccharide containing at least 10 residues is sufficient to span them. A docking model of PTN bound to a heparin dp12 oligosaccharide is shown in Figure 7. The model was constructed by docking a heparin dp12 oligosaccharide onto the three sites using distance constraints designed to place the reducing end at cluster 2 of the CTD. It should be noted that the PRE data indicate the opposite orientation is also possible. The docked structure was then allowed to relax in an unconstrained 450-ns molecular dynamics simulation. A tabulation of the RMSF of the

protein backbone and oligosaccharide heavy atoms show that the structure stabilized after about 200 ns of simulation, and the only significant change beyond 200 ns was a movement in the reducing end of the oligosaccharide away from cluster 2, which took place at around 400 ns in the simulation (Figure 7A). A representative frame from the trajectory after 310 ns of simulation is shown in Figure 7B. It shows the two TSR domains are aligned along the GAG oligosaccharide axis and all basic amino acids in those three sites are in a position to have favorable contacts with the GAG. This model implies that PTN's high affinity for GAG lies in its ability to utilize both domains and data from this report should be useful in elucidating the interaction between the domains and GAG.

## Supplementary Material

Refer to Web version on PubMed Central for supplementary material.

## Acknowledgments

We thank Drs. Brian Cherry and Samrat Amin of the Magnetic Resonance Research Center at Arizona State University for the maintenance of NMR spectrometers, Dr. Andre Bobkov of Sanford Burnham Prebys Medical Discovery Institute for performing the ITC experiments. This study is funded by grants from NIGMS/NIH (GM118518) and NCI/NIH (CA221235).

## Abbreviations:

| | |
|---|---|
| **CS** | chondroitin sulfate |
| **DS** | dermatan sulfate |
| **GAG** | glycosaminoglycan |
| **GalNAc** | N-acetylgalactosamine |
| **GlcNAc** | N-acetylglucosamine |
| **GlcA** | glucuronic acid |
| **IdoA** | iduronic acid |
| **HSQC** | heteronuclear single quantum coherence |
| **NTD** | N-terminal domain |
| **CTD** | C-terminal domain |
| **PTN** | pleiotrophin |
| **PTPRZ** | receptor-type protein tyrosine phosphatase ζ |
| **RMSF** | root mean square fluctuation |
| **TSR** | Thrombospondin type-1 repeat |

## Reference


[1]. Paveliev M et al. (2016). HB-GAM (pleiotrophin) reverses inhibition of neural regeneration by the CNS extracellular matrix. Sci Rep 6, 33916. [PubMed: 27671118]

[2]. Rauvala H (1989). An 18-kd heparin-binding protein of developing brain that is distinct from fibroblast growth factors. EMBO J 8, 2933–41. [PubMed: 2583087]

[3]. Alsmadi NZ et al. (2018). Glial-derived growth factor and pleiotrophin synergistically promote axonal regeneration in critical nerve injuries. Acta Biomater 78, 165–177. [PubMed: 30059799]

[4]. Lamprou M, Kaspiris A, Panagiotopoulos E, Giannoudis PV and Papadimitriou E (2014). The role of pleiotrophin in bone repair. Injury 45, 1816–23. [PubMed: 25456495]

[5]. Li G, Bunn JR, Mushipe MT, He Q and Chen X (2005). Effects of pleiotrophin (PTN) over-expression on mouse long bone development, fracture healing and bone repair. Calcif Tissue Int 76, 299–306. [PubMed: 15812580]

[6]. Li J et al. (2007). The pro-angiogenic cytokine pleiotrophin potentiates cardiomyocyte apoptosis through inhibition of endogenous AKT/PKB activity. J Biol Chem 282, 34984–93. [PubMed: 17925408]

[7]. Ochiai K, Muramatsu H, Yamamoto S, Ando H and Muramatsu T (2004). The role of midkine and pleiotrophin in liver regeneration. Liver Int 24, 484–91. [PubMed: 15482347]

[8]. Gu D, Yu B, Zhao C, Ye W, Lv Q, Hua Z, Ma J and Zhang Y (2007). The effect of pleiotrophin signaling on adipogenesis. FEBS Lett 581, 382–8. [PubMed: 17239862]

[9]. Sevillano J et al. (2019). Pleiotrophin deletion alters glucose homeostasis, energy metabolism and brown fat thermogenic function in mice. Diabetologia 62, 123–135. [PubMed: 30327824]

[10]. Yi C et al. (2011). MiR-143 enhances adipogenic differentiation of 3T3-L1 cells through targeting the coding region of mouse pleiotrophin. FEBS Lett 585, 3303–9. [PubMed: 21945314]

[11]. Yokoi H et al. (2012). Pleiotrophin triggers inflammation and increased peritoneal permeability leading to peritoneal fibrosis. Kidney Int 81, 160–9. [PubMed: 21881556]

[12]. Heroult M et al. (2004). Heparin affin regulatory peptide binds to vascular endothelial growth factor (VEGF) and inhibits VEGF-induced angiogenesis. Oncogene 23, 1745–53. [PubMed: 15001987]

[13]. Kokolakis G, Mikelis C, Papadimitriou E, Courty J, Karetsou E and Katsoris P (2006). Effect of heparin affin regulatory peptide on the expression of vascular endothelial growth factor receptors in endothelial cells. In Vivo 20, 629–35. [PubMed: 17091770]

[14]. Koutsioumpa M et al. (2012). Pleiotrophin expression and role in physiological angiogenesis in vivo: potential involvement of nucleolin. Vasc Cell 4, 4. [PubMed: 22423616]

[15]. Papadimitriou E, Pantazaka E, Castana P, Tsalios T, Polyzos A and Beis D (2016). Pleiotrophin and its receptor protein tyrosine phosphatase beta/zeta as regulators of angiogenesis and cancer. Biochim Biophys Acta 1866, 252–265. [PubMed: 27693125]

[16]. Poimenidi E, Theodoropoulou C, Koutsioumpa M, Skondra L, Droggiti E, van den Broek M, Koolwijk P and Papadimitriou E (2016). Vascular endothelial growth factor A (VEGF-A) decreases expression and secretion of pleiotrophin in a VEGF receptor-independent manner. Vascul Pharmacol 80, 11–9. [PubMed: 26924457]

[17]. Peria FM et al. (2007). Pleiotrophin expression in astrocytic and oligodendroglial tumors and it's correlation with histological diagnosis, microvascular density, cellular proliferation and overall survival. J Neurooncol 84, 255–61. [PubMed: 17443289]

[18]. Shi Y et al. (2017). Tumour-associated macrophages secrete pleiotrophin to promote PTPRZ1 signalling in glioblastoma stem cells for tumour growth. J Clin Pathol 8, 15080.

[19]. Zhang L et al. (2015). Pleiotrophin promotes vascular abnormalization in gliomas and correlates with poor survival in patients with astrocytomas. Sci Signal 8, ra125. [PubMed: 26645582]

[20]. Maeda N, Nishiwaki T, Shintani T, Hamanaka H and Noda M (1996). 6B4 proteoglycan/phosphacan, an extracellular variant of receptor-like protein-tyrosine phosphatase zeta/RPTPbeta, binds pleiotrophin/heparin-binding growth-associated molecule (HB-GAM). J Biol Chem 271, 21446–52. [PubMed: 8702927]

[21]. Raulo E, Chernousov MA, Carey DJ, Nolo R and Rauvala H (1994). Isolation of a neuronal cell surface receptor of heparin binding growth-associated molecule (HB-GAM). Identification as N-syndecan (syndecan-3). J Biol Chem 269, 12999–3004. [PubMed: 8175719]

[22]. Take M, Tsutsui J, Obama H, Ozawa M, Nakayama T, Maruyama I, Arima T and Muramatsu T (1994). Identification of nucleolin as a binding protein for midkine (MK) and heparin-binding growth associated molecule (HB-GAM). J Biochem 116, 1063–8. [PubMed: 7896734]

[23]. Koutsioumpa M et al. (2013). Interplay between alphavbeta3 integrin and nucleolin regulates human endothelial and glioma cell migration. J Biol Chem 288, 343–54. [PubMed: 23161541]

[24]. Shen D, Podolnikova NP, Yakubenko VP, Ardell CL, Balabiyev A, Ugarova TP and Wang X (2017). Pleiotrophin, a multifunctional cytokine and growth factor, induces leukocyte responses through the integrin Mac-1. 292, 18848–18861.

[25]. Varki A (2009) Essentials of glycobiology, Cold Spring Harbor Laboratory Press. Cold Spring Harbor, N.Y.

[26]. Lindahl U, Backstrom G, Thunberg L and Leder IG (1980). Evidence for a 3-O-sulfated D-glucosamine residue in the antithrombin-binding sequence of heparin. Proc Natl Acad Sci U S A 77, 6551–5. [PubMed: 6935668]

[27]. Mizumoto S, Fongmoon D and Sugahara K (2013). Interaction of chondroitin sulfate and dermatan sulfate from various biological sources with heparin-binding growth factors and cytokines. Glycoconj J 30, 619–32. [PubMed: 23275130]

[28]. Ori A, Free P, Courty J, Wilkinson MC and Fernig DG (2009). Identification of heparin-binding sites in proteins by selective labeling. Mol Cell Proteomics 8, 2256–65. [PubMed: 19567366]

[29]. Kilpelainen I, Kaksonen M, Kinnunen T, Avikainen H, Fath M, Linhardt RJ, Raulo E and Rauvala H (2000). Heparin-binding growth-associated molecule contains two heparin-binding beta -sheet domains that are homologous to the thrombospondin type I repeat. J Biol Chem 275, 13564–70. [PubMed: 10788472]

[30]. Maeda N, Fukazawa N and Hata T (2006). The binding of chondroitin sulfate to pleiotrophin/heparin-binding growth-associated molecule is regulated by chain length and oversulfated structures. J Biol Chem 281, 4894–902. [PubMed: 16373346]

[31]. Li F, Nandini CD, Hattori T, Bao X, Murayama D, Nakamura T, Fukushima N and Sugahara K (2010). Structure of pleiotrophin- and hepatocyte growth factor-binding sulfated hexasaccharide determined by biochemical and computational approaches. J Biol Chem 285, 27673–85. [PubMed: 20584902]

[32]. Ryan E, Shen D and Wang X (2016). Structural studies reveal an important role for the pleiotrophin C-terminus in mediating interactions with chondroitin sulfate. FEBS J 283, 1488–503. [PubMed: 26896299]

[33]. Catanzariti AM, Soboleva TA, Jans DA, Board PG and Baker RT (2004). An efficient system for high-level expression and easy purification of authentic recombinant proteins. Protein Science 13, 1331–1339. [PubMed: 15096636]

[34]. Cai C, Solakyildirim K, Yang B, Beaudet JM, Weyer A, Linhardt RJ and Zhang F (2012). Semi-synthesis of chondroitin sulfate-E from chondroitin sulfate-A. Carbohydr Polym 87, 822–829. [PubMed: 22140285]

[35]. Delaglio F, Grzesiek S, Vuister GW, Zhu G, Pfeifer J and Bax A (1995). Nmrpipe - a Multidimensional Spectral Processing System Based on Unix Pipes. Journal of Biomolecular Nmr 6, 277–293. [PubMed: 8520220]

[36]. Johnson BA (2004). Using NMRView to visualize and analyze the NMR spectra of macromolecules. Methods Mol Biol 278, 313–52. [PubMed: 15318002]

[37]. Kirschner KN, Yongye AB, Tschampel SM, Gonzalez-Outeirino J, Daniels CR, Foley BL and Woods RJ (2008). GLYCAM06: a generalizable biomolecular force field. Carbohydrates. J Comput Chem 29, 622–55. [PubMed: 17849372]

[38]. Case DA et al. (2005). The Amber biomolecular simulation programs. J Comput Chem 26, 1668–88. [PubMed: 16200636]

[39]. Nieto L et al. (2013). Heparin modulates the mitogenic activity of fibroblast growth factor by inducing dimerization of its receptor. a 3D view by using NMR. Chembiochem 14, 1732–44. [PubMed: 23940086]

[40]. García-Mayoral MF et al. (2013). Insights into the glycosaminoglycan-mediated cytotoxic mechanism of eosinophil cationic protein revealed by NMR. ACS Chem Biol 8, 144–51. [PubMed: 23025322]

[41]. Deshauer C, Morgan AM, Ryan EO, Handel TM, Prestegard JH and Wang X (2015). Interactions of the Chemokine CCL5/RANTES with Medium-Sized Chondroitin Sulfate Ligands. Structure 23, 1066–77. [PubMed: 25982530]

[42]. Clore GM, Tang C and Iwahara J (2007). Elucidating transient macromolecular interactions using paramagnetic relaxation enhancement. Curr Opin Struct Biol 17, 603–16. [PubMed: 17913493]

[43]. Kojima S et al. (1997). Dimerization of midkine by tissue transglutaminase and its functional implication. J Biol Chem 272, 9410–6. [PubMed: 9083079]

[44]. Xu J and Van Doren SR (2018). Affinities and Comparisons of Enzyme States by Principal Component Analysis of NMR Spectra, Automated using TREND Software. Methods Enzymol 607, 217–240. [PubMed: 30149859]

[45]. Raulo E et al. (2005). The two thrombospondin type I repeat domains of the heparin-binding growth-associated molecule bind to heparin/heparan sulfate and regulate neurite extension and plasticity in hippocampal neurons. J Biol Chem 280, 41576–83. [PubMed: 16155004]

[46]. Solera C, Macchione G, Maza S, Kayser MM, Corzana F, de Paz JL and Nieto PM (2016). Chondroitin Sulfate Tetrasaccharides: Synthesis, Three-Dimensional Structure and Interaction with Midkine. Chemistry 22, 2356–69. [PubMed: 26784281]

[47]. Dragan AI, Read CM and Crane-Robinson C (2017). Enthalpy–entropy compensation: the role of solvation. European Biophysics Journal 46, 301–308. [PubMed: 27796417]

[48]. Privalov PL, Dragan AI and Crane-Robinson C (2011). Interpreting protein/DNA interactions: distinguishing specific from non-specific and electrostatic from non-electrostatic components. Nucleic Acids Research 39, 2483–2491. [PubMed: 21071403]

[49]. Lu KV et al. (2005). Differential induction of glioblastoma migration and growth by two forms of pleiotrophin. J Biol Chem 280, 26953–64. [PubMed: 15908427]

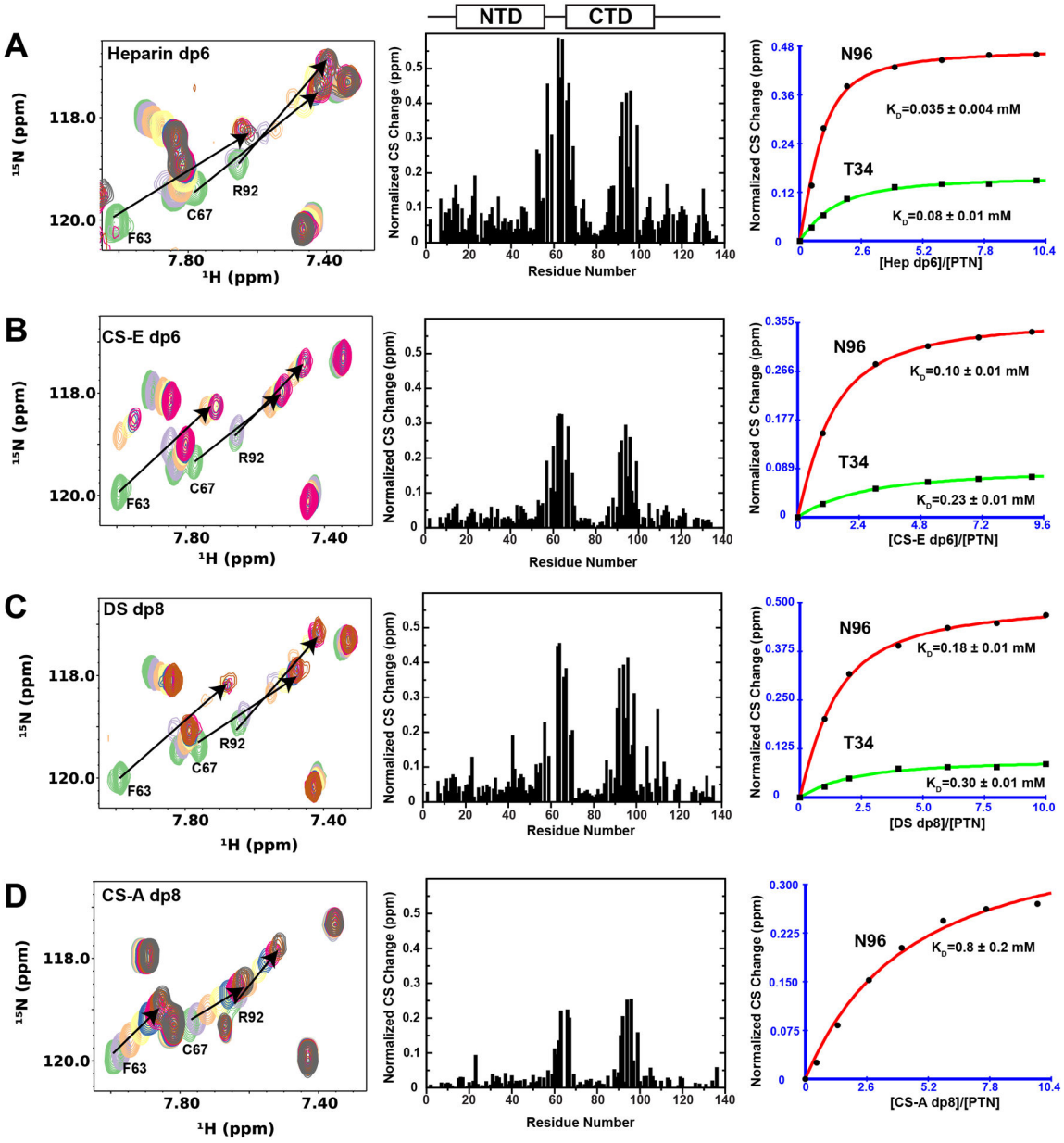


**Figure 1.**

Interactions of PTN with heparin, CS-E, DS, and CS-A oligosaccharides. A) $^{15}$N-HSQC of PTN in the presence of different concentrations of heparin dp6 are shown on the left. The maximum heparin dp6-induced chemical shift migration for each residue is shown in the bar chart in the middle. Binding curves of N96 (red) and T34 (green) are shown on the right. Heparin dp6 concentrations in the HSQCs were 0 (lime green), 0.05 (purple), 0.1 (tan), 0.2 (yellow), 0.4 (blue), 0.6 (red), 0.8 (brown), and 1.0 (grey) mM. B) Similar data for CS-E dp6. CS-E dp6 concentrations in the HSQCs were 0 (lime green), 0.125 (purple), 0.375 (tan), 0.625 (yellow), 0.875 (blue), and 1.125 mM (red). C) Similar data for DS dp8. DS dp8 concentrations in the HSQCs were 0 (lime green), 0.2 (purple), 0.4 (tan), 0.8 (yellow), 1.2 (blue), 1.6 (red), and 2.0 (brown) mM. D) Similar data for CS-A

dp8. CS-A dp8 concentrations in the HSQCs were 0 (lime green), 0.09 (purple), 0.26 (tan), 0.51 (yellow), 0.77 (blue), 1.11 (red), 1.45 (brown), and 1.87 (grey) mM. CS-A dp8 did not induce significant chemical shift changes in T34.

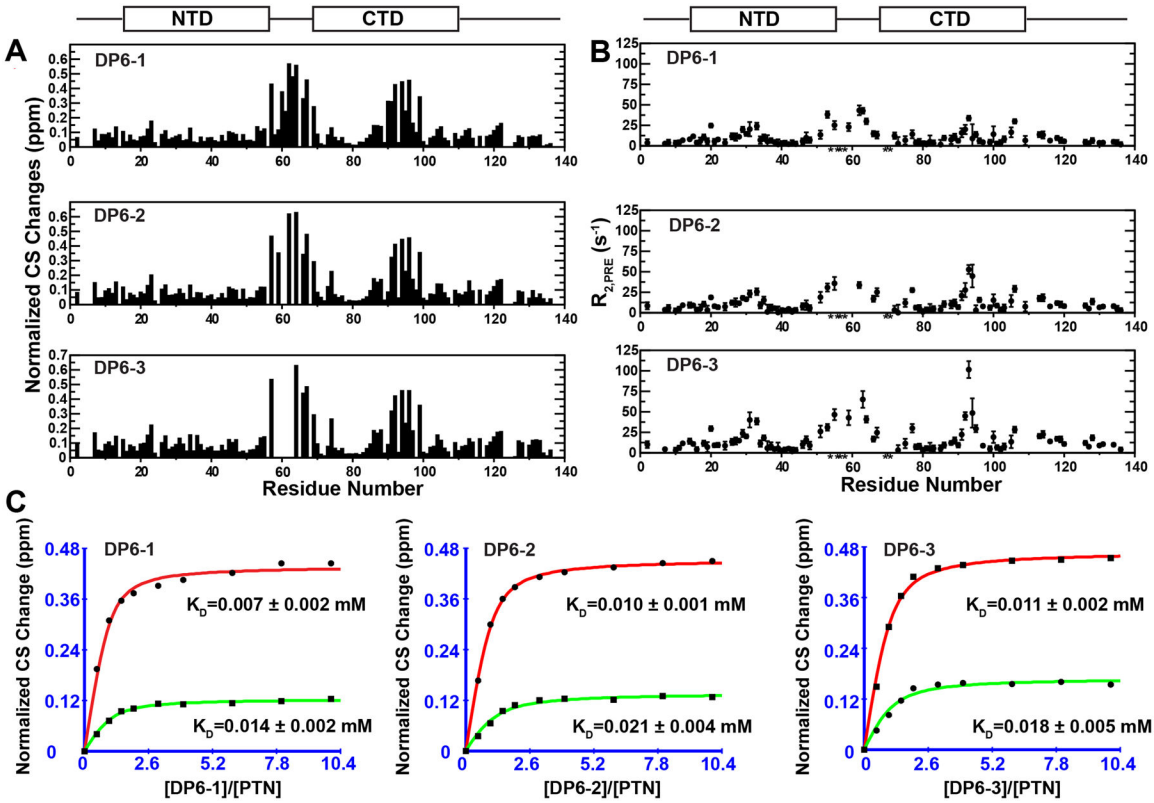


**Figure 2.**

Effects of structurally defined heparin dp6 on PTN. A) Chemical shift perturbation on $^{15}$N-HSQC of PTN by DP6-1 (ΔUA2S-GlcNS6S-IdoA-GlcNAc6S-GlcA-GlcNS6S3S), DP6-2 (ΔUA2S-GlcNS6S-IdoA2S-GlcNS6S-GlcA-GlcNS6S), and DP6-3 (ΔUA2S-GlcNS6S-IdoA2s-GlcNS6S-IdoA2s-GlcNS6S). B) PRE induced by structurally defined heparin dp6 on backbone amide hydrogens of PTN. Residue whose intensity was beyond detection in the presence of paramagnetic ligands but recovered after the reduction of the paramagnetic ligands are marked with an asterisk. C) Binding curves of N96 (CTD) and T34 (NTD).

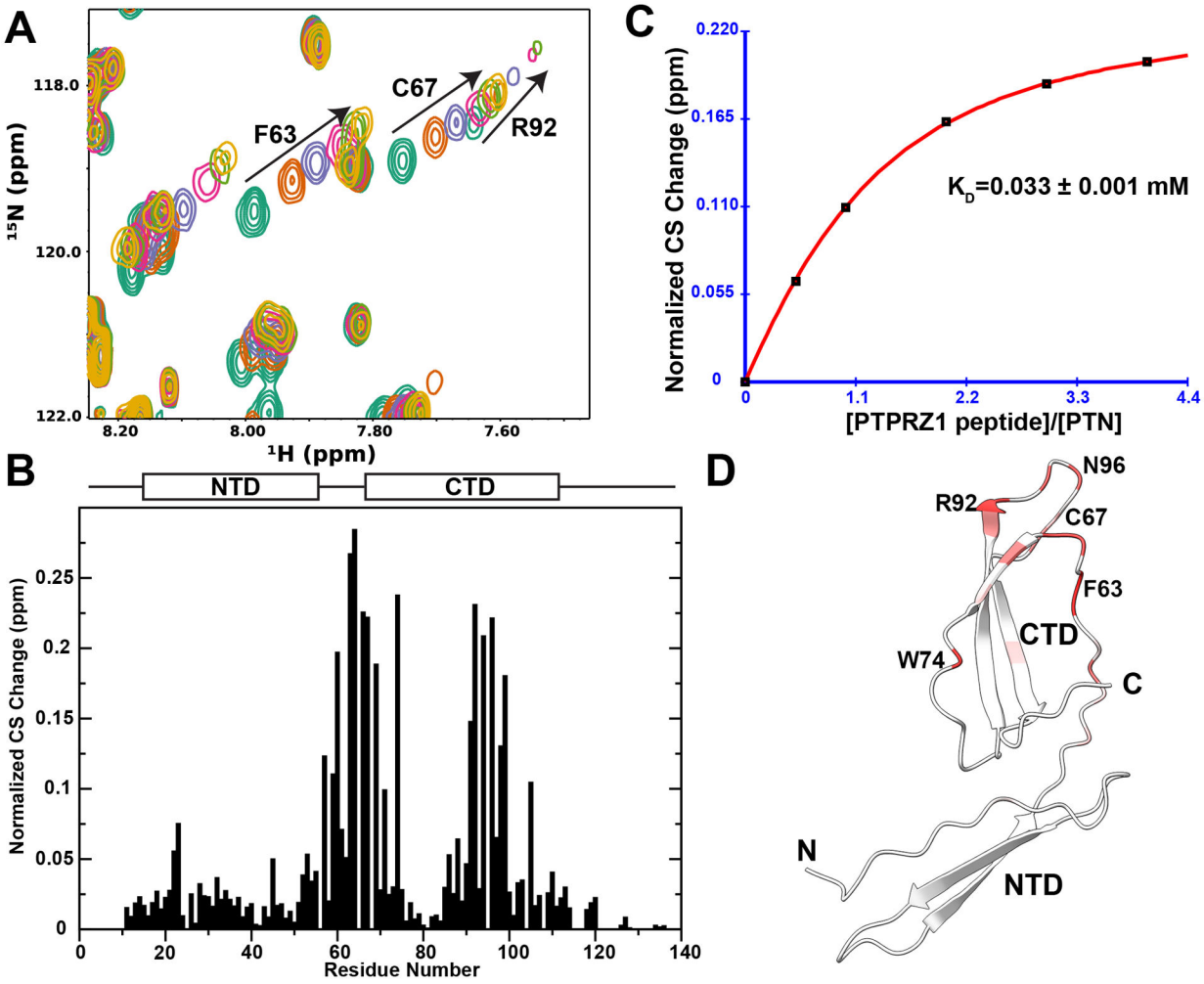


**Figure 3.**

Effects of the PTPRZ peptide (G1414-K1441) on PTN. A) PTPRZ peptide induced changes in the $^{15}$N-HSQC of PTN. PTPRZ peptide concentrations in the HSQCs were 0 (green), 25 (brown), 50 (blue), 100 (magenta), 150 (light green), and 200 (gold) μM. PTN concentration was 50 μM. B) Chemical shift changes induced by the PTPRZ peptide in the $^{15}$N-HSQC of PTN. C) Binding curve of N96 from the CTD. D) Ribbon representation of PTN where the residues are colored by a white-to-red gradient to indicate the magnitude of chemical shift change. The range of the gradient is 0.05ppm (white) to 0.25ppm (red).

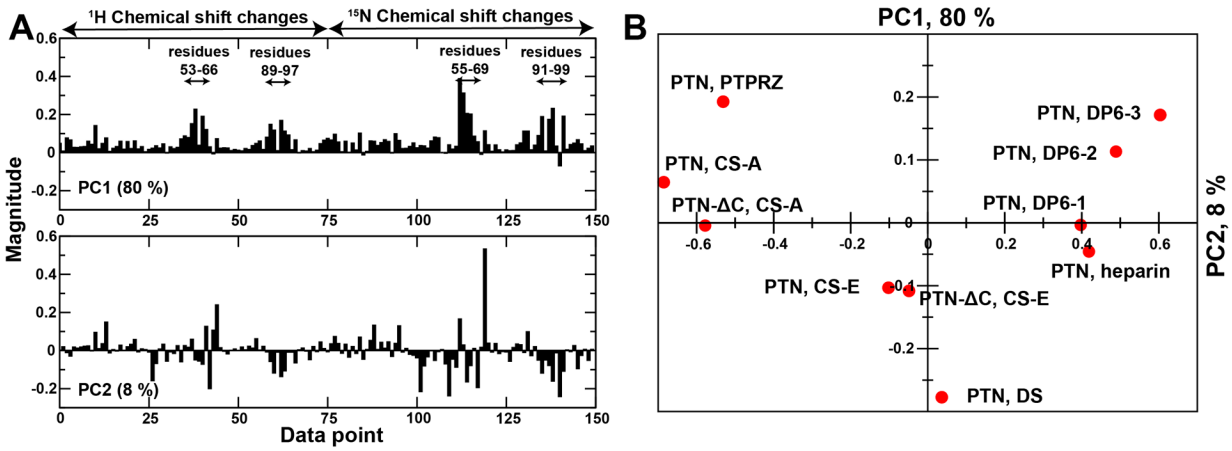


**Figure 4.**

Global analysis of GAG-induced chemical shift migrations by PCA. A) Coefficients of the two largest principal components. PC1 accounts for ~ 80 % of variance while PC2 accounts for 8 % of the variance. Data from residues experiencing large chemical shift changes in all the titrations are major components in PC1. B) Score plot of the titration data sets. Each data point is labeled with the PTN variant and GAG type used in the titration. The datasets' projection along PC1 correlate approximately with the chemical shift change magnitudes and the ligand charge density.

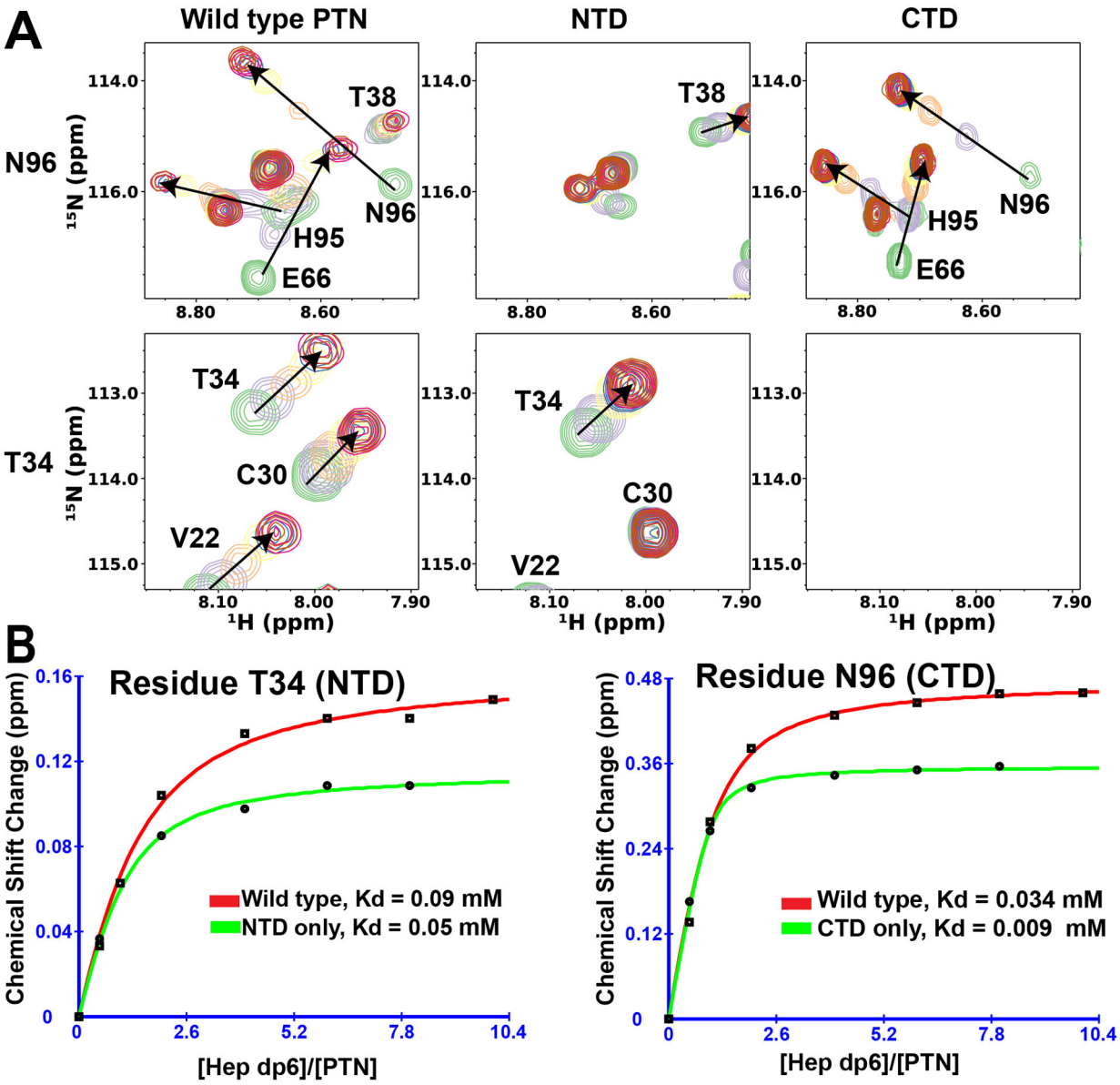


**Figure 5.**

Cooperativity of the domains in binding heparin dp6. A) Heparin dp6-induced changes in the $^{15}$N-HSQC signals of N96, T34, and other residues from wild type PTN (left), NTD (middle), and CTD (right). Concentrations of heparin dp6 in the HSQCs were 0 (lime green), 0.05 (purple), 0.1 (tan), 0.2 (yellow), 0.4 (blue), 0.6 (red), and 0.8 (brown) mM. B) Binding curves of residues T34 and N96 in wild type PTN, NTD, and CTD.

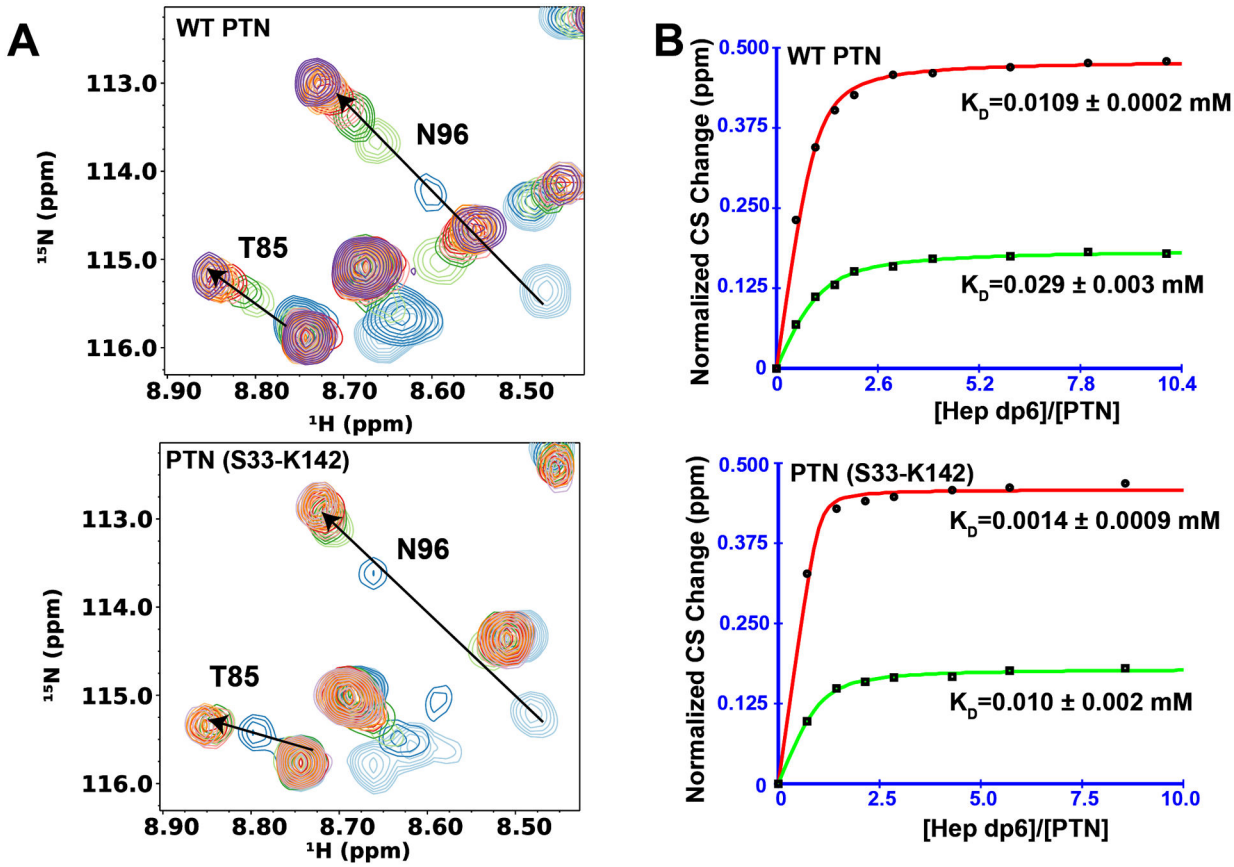


**Figure 6.**

Effects of unstructured termini on heparin dp8 affinity for the structured domains. A) $^{15}$N-HSQC of wild type PTN and PTN-ΔNC in the presence of different concentrations of heparin dp8. Heparin dp8 concentrations in the HSQCs were 0 (light blue), 0.05 (blue), 0.1 (light green), 0.15 (green), 0.2 (pink), 0.3 (red), 0.4 (gold), 0.6 (brown), 0.8 (violet), and 1.0 (purple) mM. B) Heparin dp8 binding curves of residues N96 (red) and T34 (green) from wild type PTN and PTN-ΔNC.

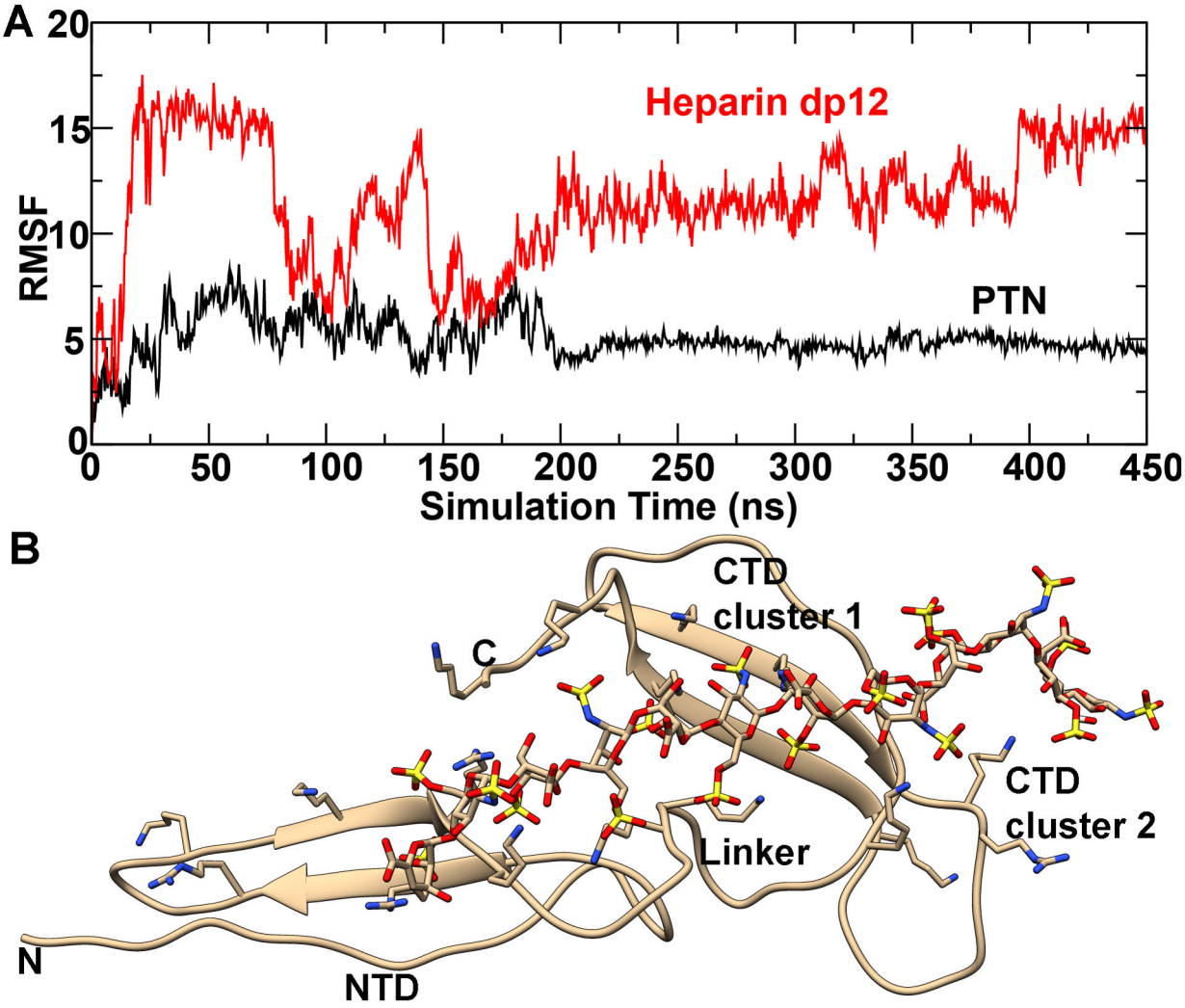


**Figure 7.**

Model of the PTN-GAG complex. A) RMSF of the PTN backbone and oligosaccharide heavy atoms during the unconstrained MD simulation. B) A frame from the trajectory at ~ 310 ns of the simulation showing PTN bound to a heparin dp12 oligosaccharide spanning all three identified GAG-binding sites.

**Table 1.**

ITC measurements of heparin dp8's interactions with wild type PTN and terminal deletion mutants.

| Variant | $K_d$ (μM)[1] | ΔH (kcal/mol)[1] | -TΔS (kcal/mol)[1] | Ligand:Protein Stoichiometry[1] |
|---|---|---|---|---|
| **WT (residues 1 – 136)** | 1.4 ± 0.1 | −1.79 ± 0.04 | −6.16 ± 0.01 | 1.08 ± 0.03 |
| **PTN-ΔN (residues 13 – 136)** | 0.8 ± 0.2 | −2.35 ± 0.04 | −5.9 ± 0.1 | 0.9 ± 0.2 |
| **PTN-ΔC (residues 1 – 114)** | 2.5 ± 0.7 | −3.4 ± 0.3 | −4.2 ± 0.5 | 1.00 ± 0.02 |
| **PTN-ΔNC (residues 13 – 114)** | 1.8 ± 0.5 | −4.3 ± 0.4 | −3.5 ± 0.0.6 | 0.7 ± 0.1 |

[1]Each experiment was performed in duplicates and the uncertainty is the standard deviation in the measurements.